Ioffe-Regel crossover for plane-wave vibrational excitations in vitreous silica

S. N. Taraskin and S. R. Elliott

Department of Chemistry, University of Cambridge, Lensfield Road, Cambridge CB2 1EW, United Kingdom
(Received 28 June 1999)

The first Ioffe-Regel crossover for vibrational plane waves (when wavelength and mean free path are comparable) has been investigated theoretically for models of vitreous silica (v-SiO_2) constructed by molecular dynamics. The crossover is found to be from a state of weak scattering to one of strong scattering, not vibrational localization. Three methods have been used to investigate the crossover: an analysis of the time evolution of a vibrational plane wave, a spectral-density analysis in frequency space, and an analysis of the final scattered state in momentum space. The first Ioffe-Regel crossover frequency is found by all three methods to be ~ 1 THz for v-SiO_2, for both longitudinal and transverse polarizations. A second Ioffe-Regel crossover occurs at ~ 6 THz for v-SiO_2, corresponding to the frequency at which the mean free path is minimal (comparable to the interatomic spacing), and the spectral-density width is maximal (comparable to the frequency range of the vibrational density of states).

I. INTRODUCTION

The scattering of classical plane waves in random media is a subject of continuing interest.[1,2] Phenomena related to this include weak localization,[1,2] Anderson localization,[3] phonon localization,[4-6] and, the subject of this paper, the Ioffe-Regel crossover[7] between weakly and strongly scattering regimes.[8,9]

As the degree of disorder in a medium increases, the scattering of a wave propagating in the medium increases and hence the mean free path l correspondingly decreases. This decrease in l cannot continue without limit. The minimum possible value of mean free path is comparable to the interatomic spacing in a solid, $l_{min} \sim a$. However, before this limit is reached, another limit is reached when the mean free path becomes comparable to the wavelength of the propagating plane-wave excitation

$$l \sim \lambda_{IR}. \qquad (1.1)$$

This is the Ioffe-Regel limit; when $l < \lambda$, a plane wave can no longer be defined. The definition given by Eq. (1.1) may be rewritten equivalently in terms of frequency as

$$\nu_{IR} \tau \sim 1, \qquad (1.2)$$

where the decay time τ of the plane wave is given by

$$\tau = lc, \qquad (1.3)$$

where c is the speed of propagation of a plane wave. It should be noted that, in the literature, definitions differing by a factor 2π are sometimes used,[10,11] e.g., $kl \sim 1$ instead of Eq. (1.1), where the wave vector $k = 2\pi/\lambda$.

Somewhat confusingly, both the conditions $l \sim \lambda_{IR}$ and $l_{min} \sim a$ have been termed the Ioffe-Regel criterion in the literature.[3,12] In order to distinguish between them, we may perhaps refer to them, respectively, as the first and second Ioffe-Regel limits. In this paper, we will mostly be concerned with the first limit.

The Ioffe-Regel criterion corresponds to a crossover in behavior from a weakly to a strongly scattering regime, as

we shall see. As a result, momentum (or equivalently the wave vector k) is no longer a good label for the propagating excitation beyond the Ioffe-Regel limit and another, equivalent, definition of the Ioffe-Regel crossover condition is when the uncertainty in wave vector is comparable to the value of the wave vector itself:

$$\Delta k \sim k_{IR}. \qquad (1.4)$$

In this paper, we obtain theoretical estimates for the Ioffe-Regel crossover frequency for both longitudinal and transverse vibrational plane-wave excitations propagating in simulated models of vitreous silica by investigating the behavior in both time and frequency domains, using Eq. (1.2) as the definition, and in **k** space using Eq. (1.4) as the relevant definition.

The rest of the paper is arranged in the following manner. Section II briefly describes the possible ways of investigating the Ioffe-Regel crossover. Estimates of the Ioffe-Regel crossover parameters, obtained from spectral-density peak widths and a temporal-decay method, are given in Sec. III and Sec. IV, respectively. An identification of the Ioffe-Regel crossover from a consideration of the final state is given in Sec. V. Discussion and conclusions are presented in Secs. VI and VII.

II. BASIC METHOD

The vibrational behavior of simulated models of vitreous silica in the vicinity of the Ioffe-Regel crossover was investigated in the harmonic approximation by means of a normal-mode analysis using the methods described in detail in the preceding accompanying paper,[13] hereafter termed paper I.

An initial plane-wave vibrational excitation (in practice, a standing wave), of a given polarization type, wave vector, and frequency, is scattered by the disordered structure into a different final state. The decay time τ of the scattering process found from the temporal decay of the initial plane wave can be used to find the Ioffe-Regel condition using Eq. (1.2). Actually, in the frequency domain, the full width at half maximum Γ of the peak-shaped spectral-density function $\bar{S}_{\mathbf{k}}$

defined by Eq. (4.4) in paper I, which is the mass-weighted projection of a plane wave $\mathbf{w_k}$ given by Eq. (3.1) in paper I, onto the vibrational eigenmodes, can also be used to obtain an estimate for τ, i.e., $\tau_k^{-1} \simeq \pi \Gamma_\nu(k)$ [see Eq. (4.9) in paper I], for a particular value of wave vector k of the initial plane wave.

The scattering process involving the initial plane (standing) wave can also be analyzed in $\mathbf{k}$ space in terms of the properties of the final state, averaged over time as $t \to \infty$. The quantity of interest is the distribution $\rho(\mathbf{k}', \hat{\mathbf{n}}' | \mathbf{k}, \hat{\mathbf{n}})$ [see Eq. (6.2) in paper I] of the time-averaged weights of different plane-wave components $\{\mathbf{k}', \hat{\mathbf{n}}'\}$, characterized by wave vector $\mathbf{k}'$ and unit polarization vector $\hat{\mathbf{n}}'$, in the final state originating from an initial state $\{\mathbf{k}, \hat{\mathbf{n}}\}$. The Ioffe-Regel limit can be determined by investigating the widths of the peaks in $\rho(\mathbf{k}', \hat{\mathbf{n}}' | \mathbf{k}, \hat{\mathbf{n}})$.

III. FREQUENCY DOMAIN

In disordered structures, and for small values of the wave-vector magnitude ($ka \ll 1$), the spectral density for both longitudinal and transverse polarizations has the shape of a single pronounced peak.[13] The peak position gives the average frequency $\bar{\nu}_k$ of the propagating excitation, and the peak width is associated with the decay time τ_k of the excitation [see Eq. (4.7) in paper I]. With increasing wave vector (or frequency), the peak width $\Gamma_\nu(k)$ increases[13] and hence τ_k decreases until the Ioffe-Regel limit [Eq. (1.2)] is reached. Fits to the peak shape of the spectral density using both Lorentzian and damped harmonic oscillator[14] functions give rather similar results[13] for $\bar{\nu}_k$ and τ_k.

The Ioffe-Regel crossover wave vector k_{IR} is found from the intersection of the two curves $\tau_k^{-1}(k)$ vs k and $\bar{\nu}_k(k)$ vs k according to Eq. (1.2). Figures 1(a) and 1(b) show such plots for transverse and longitudinal initial plane waves. The calculated dispersion curves $\bar{\nu}_k(k)$ show the expected linear dependences (dashed lines in Fig. 1) in the Ioffe-Regel crossover region. The k dependence of the inverse decay time, $\tau_k^{-1}(k)$, exhibits a quadratic behavior for $k \gtrsim 0.3$ Å^{-1}, but not exactly in the Ioffe-Regel crossover region. This discrepancy is a finite-size effect due to a limited size of the simulation box; the density of modes is rather sparse at the lowest frequencies and, as a result, the spectral density is insufficiently wide (not enough eigenmodes in this regime) and hence τ_k^{-1} is too small. In order to avoid this shortcoming of the simulated results, we extrapolated to low frequencies the quadratic behavior (solid lines in Fig. 1), as found experimentally using a variety of techniques.[14–17]

The Ioffe-Regel crossover wave vectors are estimated from the intersection point of the solid and dashed lines in Fig. 1. The values thus obtained are $k_{IR,t} \simeq 0.15$ Å^{-1} and $k_{IR,l} \simeq 0.1$ Å^{-1} for transverse and longitudinal polarizations, respectively, of the initial plane-wave excitations. Using the experimental transverse and longitudinal sound velocities in v-SiO$_2$,[14,18] viz. $c_t \simeq 37.5$ Å/ps and $c_l \simeq 59$ Å/ps, respectively, with which the simulated results are in very good agreement at low frequencies,[13] the Ioffe-Regel crossover frequency ($\nu_{IR} = c k_{IR}/2\pi$) is found to be $\nu_{IR,t} \simeq \nu_{IR,l} \simeq 1$ THz for both polarizations. The mean free path of the propagating plane-
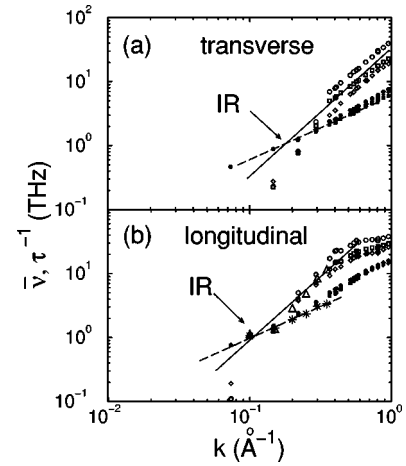

FIG. 1. The average frequency $\bar{\nu}$ (solid symbols) and inverse relaxation time τ^{-1} (open symbols) of transverse (a) and longitudinal (b) initial plane waves versus the initial wave-vector magnitude. The circles and squares are obtained from fits of the spectral densities by the DHO model and Lorentzians, respectively, as described in Sec. III. The diamonds are obtained by the temporal-decay method. The open triangles and stars in (b) represent IXS data (Ref. 14). The crossing points of the solid lines corresponding to the quadratic dependence of τ^{-1} on k and the dashed lines referring to the linear dependence of $\bar{\nu}_k$ on k mark the (first) Ioffe-Regel crossover.

wave excitations at the Ioffe-Regel limit is given by $l_{IR,t(l)} \simeq \lambda_{IR,t(l)}$, or $l_{IR,t(l)} \simeq c_{t(l)}/\nu_{IR,t(l)} \sim 2\pi/k_{IR,t(l)}$, and is estimated to be $l_{IR,t} \simeq 42$ Å for transverse and $l_{IR,l} \simeq 63$ Å for longitudinal polarizations. Note that these results are correct for not very low temperatures, $T \gtrsim 100$ K, where the decay time is temperature independent (see Ref. 11).

The common frequency dependence of the inverse decay time for both longitudinal and transverse polarizations of the initial plane-wave excitations is clearly seen in a joint plot of $\tau^{-1}(\nu)$ vs ν (Fig. 2). The quadratic dependence of $\tau^{-1}(\nu)$ vs ν is evident in the experimental data. The Ioffe-Regel
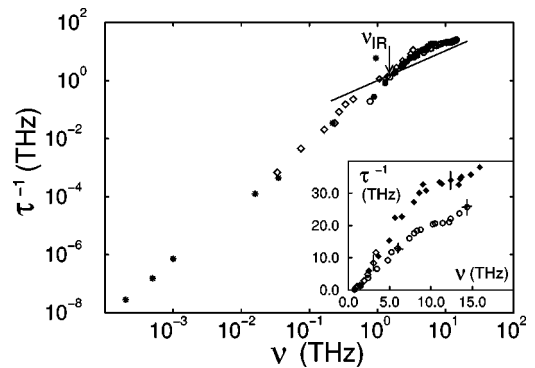

FIG. 2. The inverse decay time vs frequency of plane waves that are longitudinal (open circles and squares are for the bar and cubic models) and transverse (solid circles and squares), together with experimental data taken from Ref. 10 (stars) and from Ref. 14 (diamonds). The straight line is the curve $\tau^{-1} = \nu$. The values of τ^{-1} versus frequency of the initial plane wave obtained by the temporal-decay method (open circles) and from the fit of the spectral densities by the DHO model function (solid diamonds) are given in the inset.

crossover frequency is found as the intersection of the two curves $\tau^{-1}(\nu)$ vs ν and $\tau^{-1} = \nu$. It can be seen that $\nu_{\text{IR,t}} \simeq \nu_{\text{IR,l}} \simeq 1$ THz.

IV. TIME DOMAIN

Analysis of the peak widths of the spectral densities provides indirect estimates of the decay time of propagating plane-wave excitations. However, a more straightforward way to obtain this quantity is to calculate directly the time dependence of the amplitude $a_{\mathbf{kk}}(t)$ of the atomic displacement vector $\mathbf{u}_{\mathbf{kk}}(t)$ [see Eq. (3.7) in paper I] which is defined by Eq. (5.4) in paper I. Details of this procedure are given in paper I, together with a general method for obtaining $\bar{\nu}_k$ from the phase $\phi_{\mathbf{kk}}(t)$, even in the case of rather broad and featureless spectral densities.

The results for τ_k^{-1} obtained by this temporal-decay method are shown as the diamonds in Fig. 1 and as open circles in the inset to Fig. 2. It can be seen that there is good agreement with the results obtained from the spectral-density analysis in the Ioffe-Regel crossover region, although deviations occur at higher k or ν. Thus the estimates for k_{IR} and ν_{IR} obtained by the temporal-decay method are the same as those obtained by analysis of the spectral densities in the frequency domain.

V. MOMENTUM SPACE

The analysis of all $\mathbf{k}'$-plane-wave components in the final scattered state, in particular the distribution $\rho(\mathbf{k}',\hat{\mathbf{n}}'|\mathbf{k},\hat{\mathbf{n}})$ [see Eq. (6.1) in paper I] of their weights, allows the nature of the Ioffe-Regel regime to be clarified, the Ioffe-Regel parameters to be found and an understanding gained of why the crossover frequencies are identical (see Fig. 2) for both types of polarizations of the initial wave.

The distribution function $\rho(\mathbf{k}',\hat{\mathbf{n}}'|\mathbf{k},\hat{\mathbf{n}})$ can be calculated for the simulated models of $v\text{-SiO}_2$, and the results for the bar-shaped structural model were given in paper I. Such a model is effectively one dimensional and has restrictions for the available initial $\mathbf{k}$ and final $\mathbf{k}'$ vectors, which are mainly directed along the bar in the low-k limit. This also restricts the number of the scattering channels. In order to check the influence of the dimensionality of the model on the scattering of plane waves, we have performed a similar analysis for a cubic (three-dimensional) model of $v\text{-SiO}_2$. The results for the distribution fuctions are presented in Fig. 3. As follows from Fig. 3, we have not found any influence of the dimensionality of the model for the available wave-vector magnitudes $k \gtrsim 0.22$ Å^{-1} (for the cubic model). The weights shown in Fig. 3 were calculated for the plane-wave components characterized by all available $\mathbf{k}'$ vectors. Different data points at the same magnitude of the final wave vector k' in Fig. 3 correspond to different directions of $\mathbf{k}'$. These data fluctuate around average values mainly within the relative variance $\lesssim 30\%$. With this precision we can say then that the probabilities for an initial wave to be scattered in different directions are approximately the same. In other words, we could roughly interpret the scattering of plane waves in the vicinity of the Ioffe-Regel regime as being ''elastic s scattering.'' By elastic we mean that the average frequencies of initial and final waves are close to each other (see the dis-
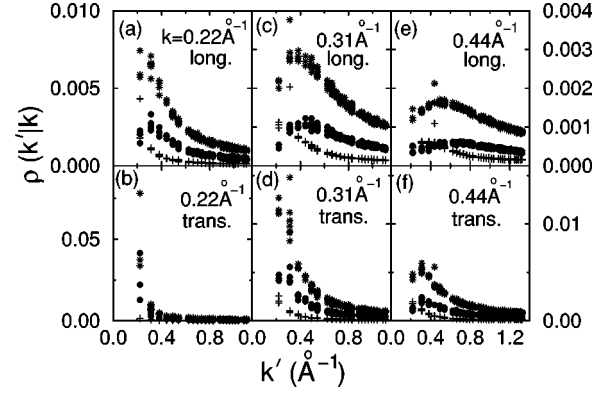

FIG. 3. The distribution functions $\rho(\mathbf{k}',\hat{\mathbf{n}}_{\text{t}}'|\mathbf{k},\hat{\mathbf{n}})$ (circles), $\rho(\mathbf{k}',\hat{\mathbf{n}}_{\text{l}}'|\mathbf{k},\hat{\mathbf{n}})$ (pluses) and $\rho_{\text{tot}}(\mathbf{k}'|\mathbf{k},\hat{\mathbf{n}})$ (stars) for longitudinal [(a), (c), and (e)] and transverse [(b), (d), and (f)] initial polarizations of plane waves characterized by different initial wave-vector magnitudes k for the cube-shaped structural model of $v\text{-SiO}_2$. The ordinate scales for (a) and (b) are on the left, and on the right for the other figures.

cussion in paper I). Note that, with increase of the initial wave-vector magnitude, there is a shift of the maxima in the distributions $\rho(\mathbf{k}',\hat{\mathbf{n}}_{\text{t}}'|\mathbf{k},\hat{\mathbf{n}}_{\text{t}})$ and $\rho(\mathbf{k}',\hat{\mathbf{n}}_{\text{l}}'|\mathbf{k},\hat{\mathbf{n}}_{\text{l}})$ to lower values as compared to k (the origin of the shift is discussed in the paper I). For example, in the case of transverse initial polarization, $\hat{\mathbf{n}} = \hat{\mathbf{n}}_{\text{t}}$ for $k \simeq 0.44$ Å^{-1}, the shift reaches the value ~ 0.1 Å^{-1}, quite comparable with the initial wave-vector magnitude [see Fig. 3(f)].

The Ioffe-Regel wave-vector parameters, as found in Secs. III and IV, are $k_{\text{IR,l}} \simeq 0.1$ Å^{-1} and $k_{\text{IR, t}} \simeq 0.15$ Å^{-1} for longitudinal and transverse initial plane waves, respectively. For our finite-size model, only a few data points are available in this range of k. Therefore the distribution functions $\rho_{\text{tot}}(\mathbf{k}'|\mathbf{k},\hat{\mathbf{n}}_{\text{t}})$ and $\rho_{\text{tot}}(\mathbf{k}'|\mathbf{k},\hat{\mathbf{n}}_{\text{l}})$ are not at all well defined in the Ioffe-Regel region. A way to overcome this shortcoming of finite-size models is discussed in the following.

The main disadvantage of finite-size simulations from the viewpoint of the present analysis is a very sparse acousticlike frequency spectrum in the low-frequency region below and around 1 THz. This is a major difficulty and can hardly be overcome by the construction of bigger models, say, realistically containing up to 10^8 particles (which are nevertheless much smaller than macroscopic values $\sim 10^{22}$). The use of an analytical approach could be very useful in this case.

Our particular interest is related to the calculation of the distribution functions of weights of different plane waves in the final state after scattering of an initial plane wave. We need to know these functions for $k \lesssim 0.1$ Å^{-1}, or equivalently for $\nu \lesssim 1$ THz, i.e., in the regions unavailable in the finite-size simulations, in order to understand what happens with these distributions in the Ioffe-Regel regime.

The distribution function defined in Eq. (6.2) of paper I can be rewritten in the following form:

$$\rho(\mathbf{k}',\hat{\mathbf{n}}'|\mathbf{k},\hat{\mathbf{n}}) \simeq 3N \int_0^\infty g(\omega)|\alpha(\omega|\mathbf{k},\hat{\mathbf{n}})|^2 |\alpha(\omega|\mathbf{k}',\hat{\mathbf{n}}')|^2 d\omega,$$

(5.1)

where for simplicity we have ignored inessential differences between the different spectral densities $|\bar{\alpha}(\omega|\mathbf{k},\hat{\mathbf{n}})|^2$
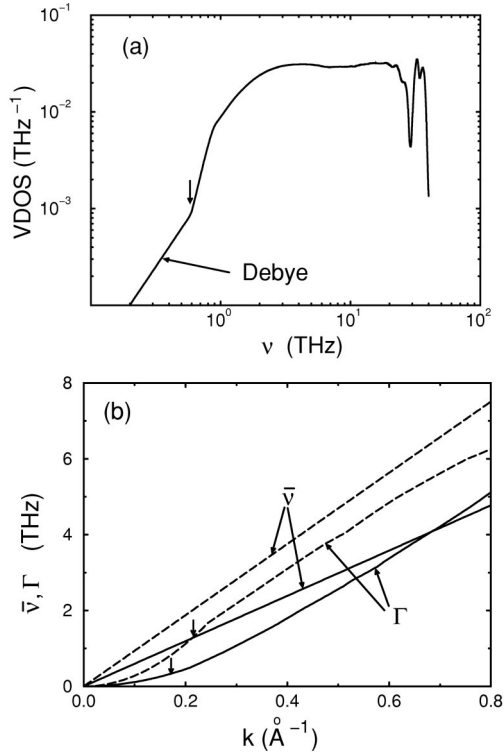
FIG. 4. (a) The VDOS and (b) the dependencies of the average frequency $\bar{\nu}$ and the peak widths Γ on the wave-vector magnitude k for transverse (solid lines) and longitudinal (dashed lines) polarizations which have been used for the integrand in Eq. (5.1). The vertical arrow in (a) shows the frequency below which the Debye law has been used for the VDOS while the vertical arrows in (b) show k values below which the quadratic law for Γ has been used.

$\equiv |\alpha(\omega|\mathbf{k},\hat{\mathbf{n}})|^2$ and $|\alpha(\omega|\mathbf{k},\hat{\mathbf{n}})|^2$ [see Eqs. (4.4)–(4.5) in paper I] and put $\langle \mathbf{w}^2_{\mathbf{k}'} \rangle \cong 1$. The integrand in Eq. (5.1) depends on the vibrational density of states (VDOS) and spectral densities. In the low-frequency regime, the VDOS is supposed to be a monotonically increasing function while the spectral densities are peak-shaped (see Fig. 11 in paper I) and the widths of the peaks decrease with decreasing frequency. If the VDOS only slightly changes on the scale of the peak width then the ω dependence of the integrand in Eq. (5.1) is mainly defined by the spectral densities and the shape of the resulting distribution function is practically independent of a particular ω dependence of the VDOS in the low-frequency regime. This is actually the case for any reasonable approximation for the VDOS as $g(\omega) \propto \omega^n$ with $n=2-4$ or $g(\omega) \propto \exp(\omega/w)$ with $w \sim 0.1$ THz if the peak width $\lesssim w$. The precise ω dependence of the VDOS in the low-frequency regime is not known and we used the Debye law as a rough estimate, $g_D(\omega) = 3\omega^2/\omega_D^3$. For $\nu \gtrsim \nu_{IR}$, the VDOS is known from simulations and experiment.[19] The resulting total VDOS's being the concatenation of these two VDOS, smoothly matching each other in the overlap region, is shown in Fig. 4(a). The use of a different ω dependence for the VDOS, e.g., $g(\omega) \propto \omega^4$ (see Ref. 20), following from the soft-potential model, does not change the shape of $\rho(\mathbf{k}',\hat{\mathbf{n}}'|\mathbf{k},\hat{\mathbf{n}})$ described below.

The important feature of the spectral densities is that they are peak shaped in the Ioffe-Regel regime and below it.
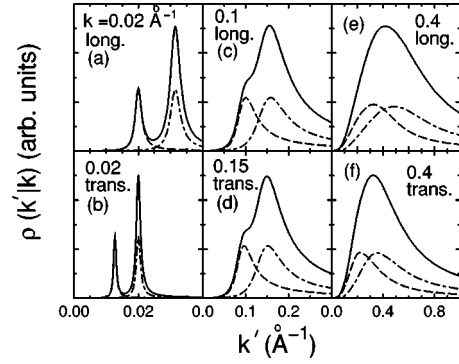

FIG. 5. The distribution functions $\rho(\mathbf{k}',\hat{\mathbf{n}}'_t|\mathbf{k},\hat{\mathbf{n}})$ (the dot-dashed lines), $\rho(\mathbf{k}',\hat{\mathbf{n}}'_l|\mathbf{k},\hat{\mathbf{n}})$ (the dashed lines) and $\rho_{tot}(\mathbf{k}'|\mathbf{k},\hat{\mathbf{n}})$ (the solid lines) for longitudinal [(a), (c), and (e)] and transverse [(b), (d), and (f)] initial polarizations of plane waves characterized by different initial wave-vector magnitudes k obtained from Eq. (5.1) with use of the VDOS and parameters for spectral densities presented in Fig. 4. Plots (c) and (d) correspond to the (first) Ioffe-Regel crossover.

These peaks can be fitted by Lorentzians and/or the damped harmonic oscillator (DHO) model (see Sec. III and paper I). The fitting functions depend on two parameters: the peak position $\nu_{t(l)}(k)$ and the peak width $\Gamma_{t(l)}(k)$. For $\nu \lesssim \nu_{IR}$, we used a linear dependence, $\nu_{t(l)}(k) = c_{t(l)}k/2\pi$, with the experimental values of sound velocities, while for $\nu \gtrsim \nu_{IR}$ the results of simulations were used [see Fig. 4(b)]. The dependence of the peak width on k for $k \lesssim k_{IR,t(l)}$, has been fitted by the experimentally found quadratic dependence, while for $k \gtrsim k_{IR,t(l)}$, the results of the simulations have been used (see Fig. 6 in paper I) so that the resulting curves are as shown in Fig. 4(b).

Once the integrand in Eq. (5.1) is defined, the distribution function $\rho(\mathbf{k}',\hat{\mathbf{n}}'|\mathbf{k},\hat{\mathbf{n}})$ can easily be found. Results for both polarizations of the initial wave are presented in Fig. 5 and should be compared with the results of the simulations shown in Fig. 3. Note that we have not performed a directional averaging for both the initial and final wave vectors in Eq. (5.1) on purpose in order to be able to compare the results with the simulation results obtained for the bar configuration (effectively a one-dimensional structure), for which such averaging in the low-k region is unavailable as well. The directional averaging of the function $\rho_{tot}(\mathbf{k}'|\mathbf{k},\hat{\mathbf{n}}) = 2\rho(\mathbf{k}',\hat{\mathbf{n}}'_t|\mathbf{k},\hat{\mathbf{n}}) + \rho(\mathbf{k}',\hat{\mathbf{n}}'_l|\mathbf{k},\hat{\mathbf{n}})$ over the final wave vector enhances the transverse peak and smooths the double-peaked structure of the distribution function because of the factor $(k')^2$ appearing in the averaging, but the function $\rho_{tot}(k'|\mathbf{k},\hat{\mathbf{n}})/(k')^2$ has the same shape as shown in Fig. 5.

Comparing Fig. 3 with Fig. 5, and Fig. 10 in the paper I, we see, not surprisingly, agreement, both qualitative and quantitative (for peak positions and their relative height), for the shapes of the curves in the case of large enough values of k (say, $k \simeq 0.4$ Å^{-1}). The advantage of the results presented in Fig. 5 as compared to those shown in Fig. 3 is that they clearly demonstrate the evolution of the distribution functions $\rho(\mathbf{k}',\hat{\mathbf{n}}'|\mathbf{k},\hat{\mathbf{n}})$ for different polarizations $\hat{\mathbf{n}}$ and $\hat{\mathbf{n}}'$ with increasing k, including the range below and around the Ioffe-Regel crossover. At any value of k under consideration, the distribution functions $\rho(\mathbf{k}',\hat{\mathbf{n}}'|\mathbf{k},\hat{\mathbf{n}})$ characterizing the indi-

vidual channels are peak-shaped (dashed and dot-dashed lines in Fig. 5). Below the Ioffe-Regel limit, these peaks are narrow and the total distributions, $\rho_{tot}(\mathbf{k'}|\mathbf{k},\hat{\mathbf{n}})$, have a double-peaked shape [see Figs. 5(a) and 5(b)]. These two peaks correspond to the two possible scattering channels for each polarization of the initial wave, i.e., $\{l \rightarrow t\}$ [the higher transverse peak in Fig. 5(a)], $\{l \rightarrow l\}$ [the lower longitudinal peak in Fig. 5(a)], and $\{t \rightarrow t\}$ [the upper transverse peak in Fig. 5(b)], and $\{t \rightarrow l\}$ [the lower longitudinal peak in Fig. 5(b)].

As follows from Eq. (5.1), the widths δk_t of the transverse peak and δk_l of the longitudinal peak in the distributions $\rho(\mathbf{k'},\hat{\mathbf{n}}'|\mathbf{k},\hat{\mathbf{n}}_t)$ and $\rho(\mathbf{k'},\hat{\mathbf{n}}'|\mathbf{k},\hat{\mathbf{n}}_l)$, respectively, are determined by the widths of the corresponding spectral densities, which depend only on the frequency of the initial plane wave but not on its polarization (see Fig. 2). Two important consequences follow from this statement. First, the widths of the transverse and longitudinal peaks in ρ are comparable, $\delta k_t \simeq \delta k_l$ (actually, we found the widths of the transverse peak to be slightly larger than the widths of the longitudinal peak for v-SiO$_2$—see Figs. 3 and 5). This is because the frequencies of the plane-wave components comprising these peaks are approximately the same and are equal to the frequency of the initial plane-wave excitation. Second, if the frequencies of the initial longitudinal and transverse waves are the same (meaning that the corresponding spectral densities are characterized by the same peak positions and approximately the same peak widths, see Fig. 2 in paper I), then they are similarly scattered by the disordered structure, i.e., the distribution functions $\rho_{tot}(\mathbf{k'}|\mathbf{k},\hat{\mathbf{n}}_t)$ and $\rho_{tot}(\mathbf{k'}|\mathbf{k},\hat{\mathbf{n}}_l)$ look similar [cf. Figs. 5(c) and 5(d) for which the frequency of the initial plane wave is the same, $\nu \simeq 1$ THz].

With increasing frequency ν or wave vector k of the initial plane wave, the peaks related to the individual channels shift to higher k' and become broader. At a certain frequency ν_{IR}, which is independent of the polarization of the initial plane-wave excitation (as discussed above), the widths of these peaks become comparable with the peak separation, $\Delta k' = k'_t - k'_l$, between longitudinal k'_l and transverse k'_t peaks in ρ_{tot}:

$$\Delta k'(\nu) \simeq \frac{c_l - c_t}{c_l} k'_t(\nu), \tag{5.2}$$

so that the Ioffe-Regel criterion in this picture is given by

$$\delta k'_t(\nu_{IR}) \simeq \delta k'_l(\nu_{IR}) \simeq \Delta k'(\nu_{IR}). \tag{5.3}$$

The total distributions $\rho_{tot}(\mathbf{k'}|\mathbf{k},\hat{\mathbf{n}}_t)$ and $\rho_{tot}(\mathbf{k'}|\mathbf{k},\hat{\mathbf{n}}_l)$, characterized by the same frequency ν_{IR}, change from having a double-peaked shape [see Figs. 5(a) and 5(b)] to a single-peak one [see Figs. 5(c) and 5(d)] with increasing k of the initial plane wave. Such a qualitative change in the shape of the total distribution of the weights of plane waves in the final state can be associated with the Ioffe-Regel crossover regime. Therefore, in this picture, condition (5.3) marks the Ioffe-Regel crossover, beyond which the final state after scattering contains many plane-wave components characterized by wave-vector magnitudes differing from the initial one by values of the order of the initial magnitude (strong-scattering regime). The wave-vector magnitude correspond-

ing to the Ioffe-Regel crossover, of course, does depend on the polarization of the initial plane wave and is determined by the sound dispersion laws

$$k_{IR,t} = 2\pi\nu_{IR}/c_t \quad \text{and} \quad k_{IR,l} = 2\pi\nu_{IR}/c_l. \tag{5.4}$$

The crossover parameters found from an analysis of the data presented in Fig. 5 using Eqs. (5.3)–(5.4) are as follows: the Ioffe-Regel frequency is $\nu_{IR} \simeq 1$ THz for both polarizations of the initial plane wave, and the corresponding wave vectors are $k_{IR,t} \simeq 0.15$ Å^{-1} for transverse and $k_{IR,l} \simeq 0.1$ Å^{-1} for longitudinal polarizations (or equivalently the corresponding mean free paths, $l_{l(t)} = c_{l(t)}\tau_{l(t)}$, are $l_{IR,t} \simeq 42$ Å and $l_{IR,l} \simeq 63$ Å). These values for ν_{IR} and k_{IR} are in excellent agreement with the experimental data[10,14] and with the estimates obtained from the analysis presented in Secs. III and IV.

VI. DISCUSSION

Our vibrational analysis of simulated models of v-SiO$_2$ has shown that the Ioffe-Regel crossover frequency for initially longitudinal plane waves is at a frequency $\nu_{IR,l} \simeq 1$ THz, in very good agreement with the same value inferred from experimental inelastic neutron-scattering data.[10] However, transverse modes are not easily probed by inelastic neutron-scattering experiments, and hence no estimate of $\nu_{IR,t}$ for v-SiO$_2$ was available before this theoretical study. Our finding that $\nu_{IR,t} \simeq \nu_{IR,l}$ implies that, concomitantly, $l_{IR,l}/l_{IR,t} \simeq c_l/c_t$, in contrast to the behavior $l_{IR,l}/l_{IR,t} \simeq (c_l/c_t)^4$ inferred previously for the case of Rayleigh scattering.[11] Such a functional relationship implies that $\tau_{IR,l}/\tau_{IR,t} \simeq (c_l/c_t)^3$ ($\simeq 3.9$ for v-SiO$_2$), rather than the equality $\tau_{IR,l} = \tau_{IR,t}$ found in this study (Fig. 2). The reason why this equality for τ_{IR} (or of ν_{IR}) should exist can be understood from a consideration of the behavior of the function $\rho(\mathbf{k'},\hat{\mathbf{n}}'|\mathbf{k},\hat{\mathbf{n}})$, as discussed in Sec. V.

The Ioffe-Regel crossover marks the (smooth) transition from weak scattering to strong scattering, as clearly evidenced by the $\mathbf{k}$ state analysis given in Sec. V. The final state after scattering, beyond the Ioffe-Regel limit, contains very many plane-wave components characterized by wave-vector magnitudes differing from the initial one by values of the order of the initial magnitude, i.e., $\Delta k \simeq k$ [see Eq. (1.4)]. However, unlike the case of electrons,[3] such strongly scattered vibrational states are not spatially localized, but instead are characteristic of a diffusive-transport regime.[21] This lack of vibrational localization at frequencies just beyond the Ioffe-Regel crossover is evident on examining the displacement amplitude of the vibrational eigenmodes;[22] such states are extended through the simulation box but certainly are not propagating plane-wave-like modes.

The frequency dependence of the inverse decay time,

$$\tau^{-1} \simeq \pi\Gamma_\nu \simeq \frac{\nu^2}{\nu_{IR}}, \tag{6.1}$$

which is just a consequence of Eq. (4.9) in paper I, the experimentally found quadratic dependence in the low-frequency range, and the definition of the Ioffe-Regel frequency given by Eq. (1.2), are not changed at the Ioffe-Regel crossover frequency, $\nu_{IR} \simeq 1$ THz (see Fig. 2). Nevertheless,

such a dependence cannot continue with further increase in frequency since there is a natural threshold for it (the ''second'' Ioffe-Regel limit). Bearing in mind that the inverse decay time is proportional to the width of the spectral density [see Eq. (6.1), we could say that this threshold is certainly less than the natural upper bound for the spectral-density width, being the width of the whole vibrational spectrum D ($D \simeq 40$ THz in silica]. In fact, the deviation from the quadratic dependence of $\tau^{-1}(\nu)$ occurs at a much lower frequency (see Fig. 2 and inset in it). This is not surprising, because we could expect an influence of the shape of the VDOS on the shape (width) of the spectral density starting with the frequency ν_{min}^* at which the width of the spectral density becomes comparable with the spectral-density peak position,

$$\Gamma_\nu(\nu_{min}^*) \simeq \nu_{min}^*, \qquad (6.2)$$

resulting in the estimate $\nu_{min}^* \simeq \pi \nu_{IR}$, i.e., at least a factor π larger than the Ioffe-Regel frequency ($\nu_{min}^* \simeq 3$ THz for silica). At the (first) Ioffe-Regel frequency, the width of the spectral density is still small enough not to destroy the quadratic dependence (6.1). Therefore we could associate the second Ioffe-Regel crossover with the frequency $\nu^* \gtrsim \nu_{min}^*$, at which the quadratic dependence of the spectral-density width (or inverse decay time) becomes modified. Examining Fig. 2 shows that in the case of vitreous silica this happens around $\nu^* \simeq 6$ THz. We believe that the second Ioffe-Regel limit corresponds to $l_{min} \simeq a$. The value of the inverse decay time at ν^* is $(\tau^*)^{-1} \simeq 15-30$ THz, this range of values resulting from different methods of estimating τ (see inset to Fig. 2). Taking the speed of sound for longitudinal acoustic waves, $c_1 \simeq 59$ Å/ps [the longitudinal branch of the curve τ^{-1} vs k shows the clearest evidence for the kink, cf. Fig. 1(b)], the corresponding mean free path is found to be $l^* = c_1 \tau^* \simeq 2-4$ Å. Thus indeed $l^* \simeq a$, since the nearest-neighbor Si-O distance d_{Si-O} in silica is about 1.6 Å.[19] It is more likely that the heights h_1 of an SiO$_4$ tetrahedron or h_2 of an SiSi$_4$ tetrahedron, respectively, are the limiting distances: $h_1 \simeq 4d_{Si-O}/3 \simeq 2.1$ Å and $h_2 \simeq 4.1$ Å (see Ref. 23). Thus this second Ioffe-Regel limit marks the onset of the random-phase-approximation regime, in which the vibrations of different SiO$_4$ and/or SiSi$_4$ tetrahedra are uncorrelated. It is significant that the spectral density of longitudinal modes starts to reach its maximum width, limited by the frequency range of the VDOS ($\simeq 40$ THz), at the wave vector $k^* \simeq 0.6$ Å^{-1} [see Fig. 2(e) in paper I] corresponding to the change in slope of curves of $\tau^{-1}(k)$ [see Fig. 6(b) in paper I].

The value of k^* can also be estimated from the phonon dispersion of the crystalline counterpart. Indeed, at $k \gtrsim k^*$, the spectral densities in α-cristobalite, the crystalline counterpart of vitreous silica, consist of many δ functions covering the whole frequency range (see Fig. 5 in paper I). This is not surprising because a typical value of Brillouin-zone boundary is $\pi/a_{u.c.} \simeq 0.5-0.6$ Å^{-1} for $a_{u.c.} \simeq 5-7$ Å, being the unit-cell size, and strong mixing between acoustic and optic modes occurs around the zone boundary. In disordered materials, the spectral density could be imagined as a superposition of broadened δ functions of the corresponding crystalline counterpart (see paper I). This also allows us to use the relationship $k^* \simeq \pi/a_{u.c.}$ for an estimate of the wave vector k^* for the second Ioffe-Regel crossover.

The frequency ν^* of the second crossover, $\nu^* = c_1 k^*/2\pi \simeq 6$ THz, of this second Ioffe-Regel limit also does not correspond to the onset of vibrational localization; examination of the participation ratio[19] shows that localization occurs only at much higher frequencies ($\nu \simeq 30$ and 40 THz) corresponding to the band edges in the VDOS of v-SiO$_2$.[19]

VII. CONCLUSIONS

The first Ioffe-Regel crossover frequency (when the mean free path and wavelength of a propagating plane-wave vibrational excitation are comparable) has been determined for simulated models of vitreous silica (v-SiO$_2$) by three methods: analysis in the time and frequency domains and in **k** space. In all cases, the Ioffe-Regel crossover frequency is found to be $\nu_{IR} \simeq 1$ THz for both longitudinal and transverse plane-wave excitations. The Ioffe-Regel limit corresponds to a crossover from a weakly scattered propagating-phonon regime to a strongly scattered diffusive-mode regime. A second Ioffe-Regel crossover is evident at a higher frequency ($\nu^* \simeq 6$ THz), which corresponds to the onset of a random-phase regime in which SiO$_4$ (or SiSi$_4$) tetrahedra vibrate incoherently and the width of the spectral density of the modes becomes comparable to its maximum value (the frequency range of the vibrational density of states). At this limit, the mean free path attains its minimum value, comparable to the interatomic spacing.

[1] *Scattering and Localization of Classical Waves in Random Media*, edited by P. Sheng (World Scientific, Singapore, 1990).

[2] P. Sheng, *Introduction to Wave Scattering, Localization, and Mesoscopic Phenomena* (Academic Press, San Diego, 1995).

[3] N. F. Mott and E. A. Davis, *Electronic Processes in Non-Crystalline Materials*, 2nd ed. (Clarendon Press, Oxford, 1979).

[4] S. John, H. Sompolinsky, and M. J. Stephen, Phys. Rev. B **27**, 5592 (1983).

[5] A. Aharony, S. Alexander, O. Entin-Wohlman, and R. Orbach, Phys. Rev. Lett. **58**, 132 (1987).

[6] S. Alexander, Phys. Rev. B **40**, 7953 (1989).

[7] A. F. Ioffe and A. R. Regel, Prog. Semicond. **4**, 237 (1960).

[8] P. Sheng, M. Zhou, and Z.-Q. Zhang, Phys. Rev. Lett. **72**, 234 (1994).

[9] E. Anglaret, A. Hasmy, E. Courtens, J. Pelous, and R. Vacher, Europhys. Lett. **28**, 591 (1994).

[10] M. Foret, E. Courtens, R. Vacher, and J.-B. Suck, Phys. Rev. Lett. **77**, 3831 (1996).

[11] R. Vacher, J. Pelous, and E. Courtens, Phys. Rev. B **56**, R481 (1997).

[12] N. F. Mott, *Conduction in Non-Crystalline Materials* (Clarendon Press, Oxford, 1987).

[13] S. N. Taraskin and S. R. Elliott, preceding paper, Phys. Rev. B **61**, 12 017 (2000).

[14] P. Benassi, M. Krisch, C. Masciovecchio, V. Mazzacurati, G. Monaco, G. Ruocco, F. Sette, and R. Verbeni, Phys. Rev. Lett. **77**, 3835 (1996).

[15] C. Masciovecchio, G. Ruocco, F. Sette, P. Benassi, A. Consulo, M. Krisch, V. Mazzacurati, A. Mermet, G. Monaco, and R. Verbeni, Phys. Rev. B **55**, 8049 (1997).

[16] T. C. Zhu, H. J. Maris, and J. Tauc, Phys. Rev. B **44**, 4281 (1991).

[17] R. Vacher, J. Pelous, F. Plicque, and A. Zarembowitch, J. Non-Cryst. Solids **45**, 397 (1981).

[18] F. Terki, C. Levelut, M. Boissier, and J. Pelous, Phys. Rev. B **53**, 2411 (1996).

[19] S. N. Taraskin and S. R. Elliott, Phys. Rev. B **56**, 8605 (1997).

[20] M. A. Il'in, V. G. Karpov, and D. A. Parshin, Zh. Eksp. Teor. Fiz. **92**, 291 (1987) [Sov. Phys. JETP **65**, 165 (1987)].

[21] J. Fabian and P. B. Allen, Phys. Rev. Lett. **77**, 3839 (1996).

[22] S. N. Taraskin and S. R. Elliott, Phys. Rev. B **59**, 8572 (1999).

[23] S. N. Taraskin and S. R. Elliott, Europhys. Lett. **39**, 37 (1997).